ACS Macro Letters

Letter

pubs.acs.org/macroletters

Enhanced Pulsatile Drug Release from Injectable Magnetic Hydrogels with Embedded Thermosensitive Microgels

Scott Campbell, Danielle Maitland, and Todd Hoare*

Department of Chemical Engineering, McMaster University, 1280 Main Street West, Hamilton, Ontario Canada L8S 4L7

Supporting Information

ABSTRACT: Nanocomposite in situ-gelling hydrogels containing both superparamagnetic iron oxide nanoparticles (SPIONs) and thermoresponsive microgels are demonstrated to facilitate pulsatile, high-low release of a model drug (4 kDa fluorescein-labeled dextran). The materials can be injected through a minimally invasive route, facilitate a ~4-fold enhancement of release when pulsed on relative to the off state, and, in contrast to previous gel-based systems, can maintain pulsatile release properties over multiple cycles and multiple days instead of only hours. Optimal pulsatile release is achieved when the microgel transition temperature is engineered to lie just above the (physiological) incubation temperature. Coupled with the demonstrated degradability of the nanocomposites and the cytocompatibility of all nanocomposite components, we anticipate these nanocomposites have potential to facilitate physiologically relevant, controlled pulsatile drug delivery.

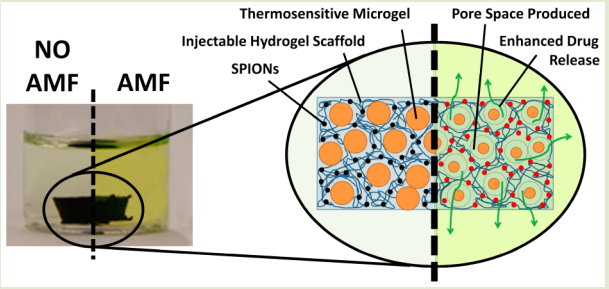

Significant progress has been made in the development of "smart" polymer-based biomaterials for the purpose of drug delivery, exploiting polymers that are responsive to temperature,[1,2] pH,[3,4] light,[5,6] electric fields,[7] or specific molecule concentrations (such as glucose)[8,9] to induce on-demand or environment-specific release kinetics. Thermoresponsive hydrogels and microgels based on temperature-responsive poly(*N*-isopropylacrylamide) (PNIPAM)[10,11] that exhibit a volume phase transition temperature (VPTT) upon heating[12] have been used to fabricate several potential drug delivery biomaterials with temperature-dependent release kinetics.[13−15] Composite materials that combine thermosensitive hydrogels with nanomaterials that generate heat in response to specific external signals, such as carbon nanotubes (near-IR),[16,17] gold nanorods (near-IR),[18−20] or superparamagnetic iron oxide nanoparticles (SPIONs, alternating magnetic field)[21,22] have attracted particular interest since the inorganic actuating nanoparticles can be used to noninvasively induce temperature-dependent swelling/deswelling responses in vivo without the need for implanted electronics.[14] The design of the nanocomposite can regulate whether release occurs via bursts of drug on-demand[23] or via an up-regulation of release kinetics over an extended period of time,[24] with up to 20-fold on/off state resolution having been reported.[24]

We have previously reported an injectable, degradable in situ-gelling hydrogel nanocomposite material in which SPIONs were covalently bound into the hydrogel network structure, fabricated by reacting aldehyde-functionalized dextran with hydrazide-functionalized PNIPAM-coated SPIONs.[25−27] The resulting hydrogel nanocomposite exhibited surprising mechanical strength (up to ~60 kPa shear modulus) and, notably, an ability to deliver pulsatile releases of drug upon the induction of an alternating magnetic field (AMF).[28] Relative to previous reports of materials or devices exhibiting pulsatile release kinetics, the in situ-gelling hydrogel approach described offers significant advantages in terms of representing an injectable, minimally invasive method of creating a bulk implant inside the body; the hydrogel portion of the material also helps to minimize nonspecific protein adsorption. However, the observed increase in drug release upon AMF application was both too small relative to the baseline in the absence of the AMF and too short-lived (i.e., exhausted in less than 1 day) for practical use in on-demand drug delivery.

Herein, we report on the use of an injectable, degradable hydrogel-thermoresponsive microgel-SPION nanocomposite hydrogel that addresses these challenges. While microgels themselves have been investigated for therapeutic delivery, they are typically quickly sequestered by the lymphatic system.[29,30] Encapsulating microgels in a hydrogel both prevents this rapid sequestration and limits the burst release of drugs typically observed from hydrogels to permit sustained release of even small molecule drugs over several weeks.[31] Furthermore, by using SPIONs as an actuator, thermosensitive microgels can be driven to deswell via externally mediated heating, generating free volume in the hydrogel to enhance drug release.

The in situ-gelling hydrogel matrix consists of thermosensitive hydrazide-functionalized PNIPAM (PNIPAM-Hzd) cross-linked with aldehyde-functionalized dextran (Dex-Ald); these materials form a hydrolytically degradable hydrazone cross-

Received: January 24, 2015
Accepted: February 17, 2015
Published: February 20, 2015

DOI: 10.1021/acsmacrolett.5b00057
ACS Macro Lett. 2015, 4, 312−316

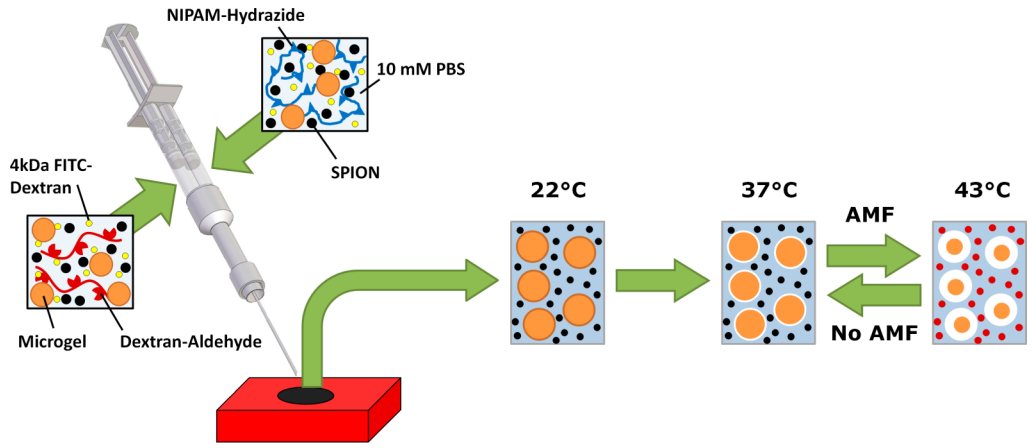

Figure 1. Fabrication of nanocomposites and their proposed mechanism of externally AMF-controlled enhanced drug release.

linked network within seconds following coextrusion from a double-barrel syringe. Two types of SPIONs were incorporated into these networks: (1) PNIPAM-Hzd functionalized SPIONs that covalently cross-link directly to the hydrogel matrix (hypothesized to enhance the mechanics and dimensional stability of the bulk gel network) and (2) polyethylene glycol (PEG)-functionalized SPIONs that are physically entrapped within the hydrogel (facilitating enhanced SPION mobility that may lead to more homogeneous heating responses). The thermoresponsive microgels were prepared by copolymerizing NIPAM with *N*-isopropylmethacrylamide (NIPMAM) to obtain microgels that exhibit a 90% decrease in volume when heated from 37 to 43 °C (i.e., from physiological temperature to the maximum temperature before which local tissue damage is observed,[32] Figure S1). These microgels are physically entrapped inside the hydrogel upon in situ gelation to form microgel-filled macropores within the bulk gel. When an AMF is applied, the heat generated by SPIONs raises the local temperature of the microgels above their VPTT, creating free volume within the composite that promotes increased drug diffusion through the hydrogel (Figure 1). Upon removal of the AMF, the microgels reswell, refilling the pores and decreasing the rate of drug release, facilitating high-low pulsatile release behavior dependent on the time over which the AMF was applied. While this mechanism has been demonstrated with bulk reservoir-based, nondegradable devices that would require surgical implantation,[24,33] such behavior has not been demonstrated with a matrix that can undergo in situ gelation upon injection from easily injectable, low-viscosity precursor components and ultimately degrades into cytocompatible materials that would have significant advantages from a practical utilization standpoint.

Composites were fabricated by mixing 10 mM PBS solutions of the reactive hydrogel precursors (8 wt % for each polymer, loaded into separate barrels of the double-barrel syringe) with 5 wt % SPIONs (loaded in both barrels), 1 wt % of 4 kDa FITC-dextran (used as the model therapeutic for tracking release, loaded in both barrels), and (if present) 8 wt % (by dry weight) microgels (loaded in both barrels; Figure 1). Thermogravimetric analysis confirmed that all final composites contained ∼5 wt % SPIONs (Figure S2), and SQUID analysis confirmed that the nanocomposite hydrogels as a whole exhibited superparamagnetic properties (Figure S3). In addition, the nanocomposites are confirmed to be degradable in accelerated hydrolysis conditions (∼240 h lifetime in pH 1 buffer, Figure S4), a similar time frame to our previously reported PNIPAM-SPION nanocomposites that degrade over ∼8 months in in vitro physiological conditions.[28]

To examine the potential of using an AMF to control release from these injectable superparamagnetic nanocomposites, samples with 5 wt % PEG-SPIONs, 8 wt % p(NIPAM-NIPMAM) microgels, and 1 wt % 4 kDa FITC-dextran were placed in our AMF apparatus that maintains a baseline temperature of 37 °C (Figure S5) and exposed to a 2 h continuous AMF application, heating the nanocomposites to an equilibrium temperature of ∼43 °C. Figure 2 shows the cumulative release of FITC-dextran from composites prepared with both microgels and PEG-SPIONs, microgels but no PEG-SPIONs, and PEG-SPIONs but no microgels.

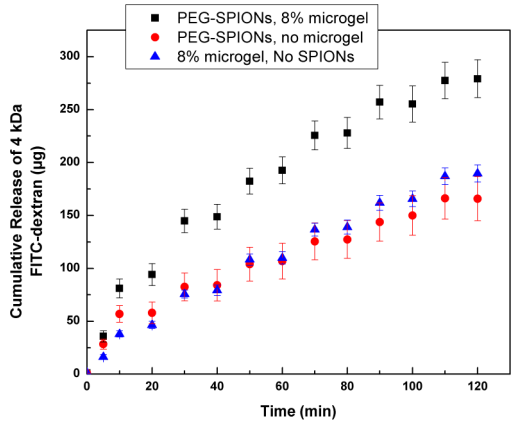

Figure 2. Cumulative release of 4 kDa FITC-dextran over 2 h of AMF exposure from a nanocomposite with 5% PEG-SPION and 8% p(NIPAM-NIPMAM) microgel content compared to control composites prepared without SPIONs and without microgel, respectively.

Significantly more release was observed from the nanocomposite prepared with both microgels and SPIONs than composites excluding either component ($p < 0.05$). Hydrogel nanocomposites lacking SPIONs do not heat significantly in response to AMF (i.e., there is no stimulus to drive microgels deswelling), while nanocomposites without microgels do heat but have no mechanism by which to generate free volume upon heating. Of note, Figure 2 indicates that the longer the AMF is left on, the more differential release can be achieved, suggesting

DOI: 10.1021/acsmacrolett.5b00057
ACS Macro Lett. 2015, 4, 312−316

the potential for dosing of a drug as a function of pulse time. Qualitatively similar behavior is also shown for the release of sodium fluorescein (Figure S6), showing that an AMF significantly enhances drug release in dual nanoparticle-based nanocomposites for drugs of significantly different molecular weights.

Pulsatile release experiments were then conducted in which the AMF was applied for a 10 min period and then shut off; the temperature of the composites increases from their baseline temperature of 37 °C to ∼43 °C over this time. A typical release result is shown in Figure S7. Significantly enhanced release of 4 kDa FITC-dextran was observed immediately after each AMF application, followed by a rapid return to a baseline release rate when AMF was shut off. While the total dose of drug decreased over time as the concentration gradient of drug was reduced, multiple AMF applications (n = 4−6) performed on days 1, 2, and 3 following composite fabrication confirm that significant pulsatile release relative to the baseline can be achieved at each time point. The AMF-induced percent increases in FITC-dextran release (relative to the nonpulsed baseline release) for composites containing cross-linked PNIPAM-SPIONs and entrapped PEG-SPIONs with and without microgels are shown in Figure 3a. The corresponding swelling responses of the nanocomposites during the time frame of the release experiment are shown in Figure 3b.

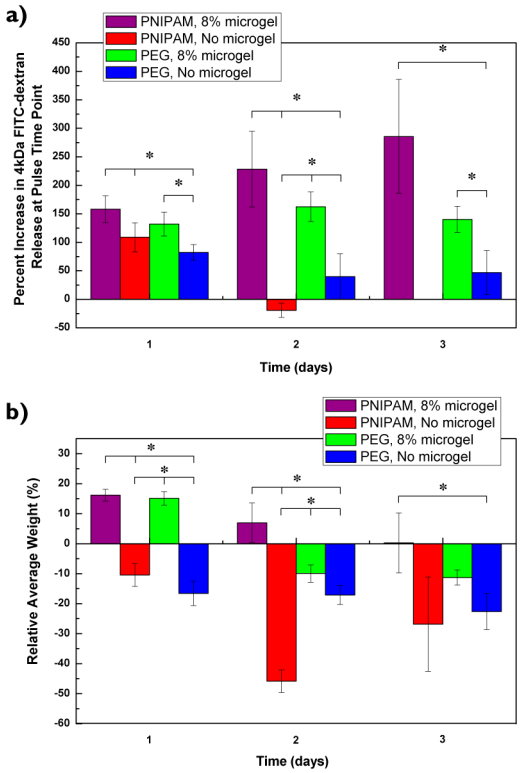

Figure 3. (a) Increase in release rate of FITC-dextran and (b) swelling characteristics for nanocomposite hydrogels prepared with PNIPAM-SPIONs and PEG-SPIONs. *p < 0.05 in a pairwise comparison.

Both composites with entrapped PEG-SPIONs and cross-linked PNIPAM-SPIONs displayed AMF-mediated enhanced release over multiple days when microgels were incorporated. The application of short AMF pulses (<10 min) resulted in a ∼4-fold increase in the release rate relative to the baseline after the first day, an enhancement that is repeatable over multiple pulsing cycles. The percentage increase in FITC-dextran release facilitated by the PEG-SPION and PNIPAM-SPION-based nanocomposites was not significantly different (p > 0.05, Figure 3a), despite the storage modulus of nanocomposites prepared with PNIPAM-SPIONs being significantly higher than that of nanocomposites based on PEG-SPIONs (p < 0.05, Figure S8); this result suggests that it is the microgel phase rather than the properties of the bulk network that primarily drives pulsatile drug release. This hypothesis is further supported by the observation that both composites prepared without microgels showed limited enhanced release after the first day, while microgel-impregnated nanocomposites continued to facilitate pulsatile release over at least 3 days (Figure 3a), which, to the best of our knowledge, is unique for any hydrogel-based system.

The macroscopic hydrogel swelling responses (Figure 3b) can be used to rationalize the differences in release behavior between nanocomposites with or without microgels. Microgel-embedded composites tend to initially swell (attributable to the higher solids fraction of the microgel relative to the bulk hydrogel phase that creates an enhanced osmotic gradient), followed by a period of deswelling as the gel equilibrates at 37 °C (attributable to PNIPAM-Hzd collapse); in contrast, nanocomposites without microgels deswell throughout the entire release period. As such, on day 1 bulk swelling would promote higher baseline (non-AMF) FITC-dextran release from the microgel-containing nanocomposites, resulting in similar observed percentage increases in FITC-dextran release relative to nanocomposites prepared without microgel despite the higher absolute values of drug release achieved on each pulse. After 1 day, the microgel-containing composites have also deswelled, reducing their baseline release to the point that the microgels (and the accompanying enhancement in nanocomposite free volume upon AMF triggering) can significantly enhance the amount of FITC-dextran released upon triggering. Nanocomposites lacking SPIONs exhibit a similar swelling response to nanocomposites prepared with both SPIONs and microgels but show no discernible increase in FITC-dextran release in response to AMF pulses, confirming that the AMF is specifically driving pulsatile release in this system (Figure S9).

To further elucidate the proposed microgel deswelling mechanism of AMF-regulated enhanced release, further pulsatile release tests were performed using the PEG-SPION composites preincubated at different baseline temperatures: room temperature (22 °C), physiological temperature (37 °C), and the maximum temperature that magnetic composites reach during AMF application (43 °C; Figure 4a). The corresponding swelling results are shown in Figure 4b.

Significantly enhanced FITC-dextran release was observed for composites incubated at 37 °C relative to the other two test temperatures upon AMF triggering. Given that the microgel experiences a 90% volume change from 37−43 °C (Figure S1), heating via AMF application will only drive a significant phase transition in the microgel phase at a 37 °C baseline temperature; nanocomposites incubated at 22 °C would not heat up enough to drive microgel deswelling while nanocomposites incubated at 43 °C would contain microgels that are already largely collapsed above their VPTT, resulting in a high, "on"-state baseline release. Figure 4b again confirms that these release kinetics results are attributable directly to microgel swelling and not bulk gel swelling, as the 22 and 43 °C baseline tests both exhibit similar, significantly lower pulsatile release kinetics (Figure 4a) but highly divergent bulk swelling

DOI: 10.1021/acsmacrolett.5b00057
ACS Macro Lett. 2015, 4, 312−316

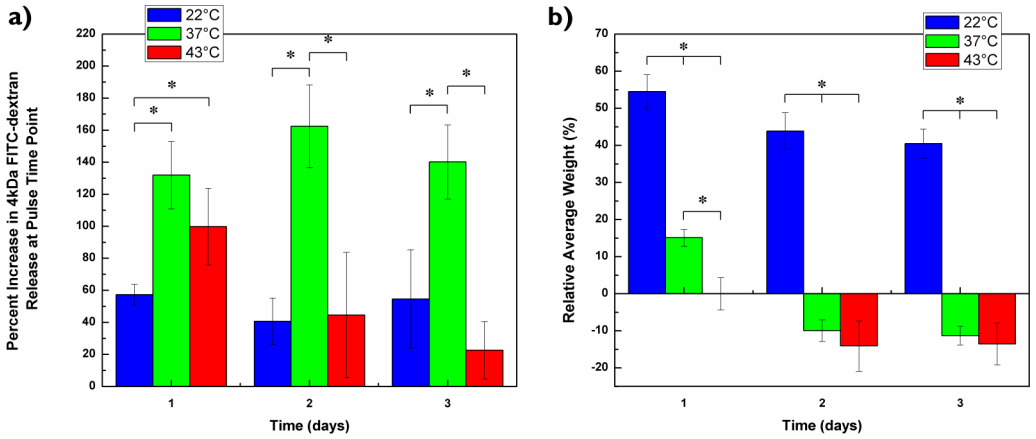

Figure 4. (a) Percentage increases in FITC-dextran release (relative to the baseline release in the absence of an AMF) and (b) relative swelling of the nanocomposites for PEG-SPION nanocomposites incubated at different baseline temperatures. $^*p < 0.05$ in a pairwise comparison.

responses (Figure 4b). Note that the relatively higher percentage increase in release observed for the 43 °C baseline test on day one is likely attributable to the large burst release observed for hydrogel composites incubated at higher temperatures.

In conclusion, incorporating thermoresponsive microgels inside injectable, degradable magnetic hydrogel composite materials significantly improves externally regulated enhanced release via an AMF. In important contrast to previous hydrogel nanocomposites, these enhancements in release persist over several days instead of just hours. AMF pulses can increase the release rate of the 4 kDa FITC-dextran model drug used herein by a factor of 4; based on our proposed release mechanism, a drug with a higher molecular weight may experience even further enhanced externally modulated release. The increase in release is related to the relationship between the baseline incubation temperature and the microgel VPTT; manipulation of both these variables may be used to create pulsatile releasing hydrogel-based nanocomposites for other, nonphysiological applications. All of the components of these nanocomposites also exhibit good cytocompatibility in vitro (Figure S10), suggesting that these materials may be promising candidates as externally controlled release platforms for a variety of different drugs in applications that would benefit from repeated, pulsatile release (e.g., chronic local pain management or insulin delivery for diabetes treatment, among others).

EXPERIMENTAL SECTION

Synthesis of Nanocomposite Components. NIPAM-Hzd was produced via copolymerization of NIPAM and acrylic acid, followed by EDC-mediated coupling of a large excess of adipic acid dihydrazide.[34] Dextran-Ald was prepared via sodium periodate-mediated oxidation of dextran.[34] Microgels were prepared by precipitation polymerization of NIPAM (36.2 mol % monomer), *N*-isopropylmethacrylamide (58.0 mol % monomer), and acrylamide (5.8 mol % monomer) using *N*,*N*-methylenebis(acrylamide) as the cross-linker and ammonium persulfate as the initiator.[33] SPIONs were prepared via redox of iron(II) chloride and iron(III) chloride salt precursor solutions using ammonium hydroxide as the base, followed by peptization of the surface with either PEG (8 kDa) or PNIPAM-Hzd at 80 °C. See Supporting Information for full protocols.

Composite Formation. Entrapped SPION hydrogel nanocomposites were fabricated by first making 10 mM PBS solutions of the reactive hydrogel precursors (8 wt % PNIPAM-Hzd in barrel 1, 8 wt % Dex-Ald in barrel 2) with 5 wt % PEG-SPIONs, 1 wt % 4 kDa FITC-dextran, and 8 wt % microgels (each added in both barrels). Final composites with 1 wt % 4 kDa FITC-dextran, 5 wt % PEG-SPIONs, and either 0 or 8 wt % microgel were produced by mixing the additives in both barrels of the double barrel syringes and ejecting the reactive cross-linking materials into silicone molds (Figure 1). The hydrogel precursors gel in situ within 30 s and the resulting nanocomposites take the shape of the silicon mold that they are placed in. Cross-linked PNIPAM-SPION-based nanocomposites were generated in a similar way, but instead, including 10 wt % PNIPAM-SPIONs in the hydrazide polymer-containing barrel only (to avoid premature cross-linking), leading to final gels with similar polymer contents and 5 wt % overall SPION contents.[28] Control composites were made similarly but excluding one component.

Physical Characterization. SPION size and morphology was characterized by transmission electron microscopy (JEOL Ltd., Japan, Figure S11). The magnetic properties of both SPIONs and nanocomposites were determined using a Superconducting Quantum Interface Device (SQUID, Quantum Design MPMS SQUID Magnetometer). Storage and loss moduli of nanocomposites were measured using an ARES parallel-plate rheometer at room temperature (1 mm sample height, 8 mm diameter), using a frequency sweep from 0.1 to 100 rad/s at a constant strain within the linear viscoelastic region of the nanocomposite ($n = 6$). Nanocomposite swelling was measured by placing 6.3 mm diameter × 3.2 mm height samples in preweighed, perforated cell culture inserts and incubating the samples in 5 mL of 10 mM PBS at 37 °C ($n = 5$). The composites were weighed immediately after gelation and then at predetermined time intervals, following the removal of nonbound (surface) water via gentle wicking with a Kimwipe, to track percentage mass change over time. Nanocomposite degradation assays were performed in a similar manner, but using samples 9.5 mm in diameter × 6.3 mm in height and replacing the 10 mM PBS with a pH 1 buffer to accelerate the rate of hydrolysis.

Drug Release Experiments. A magnetic drug release apparatus was assembled to hold multiple ($n = 4$) composites in equivalent positions within the magnetic field while maintaining a constant temperature of 37 °C (Figure S5). A jacketed flask, heated to 37 °C via a water bath for the base experiments or 22 or 43 °C for the varying temperature experiments, was placed within a 2-coiled, 8 cm diameter solenoid operated at 200 kHz, 30 A, and 1.3 kW to facilitate the application of an AMF. For the constant AMF experiments, nanocomposites ($n = 4$, 6.3 mm diameter × 3.2 mm height) were immersed in test tubes with 4 mL of 10 mM PBS and placed in the AMF for 2 h. For pulsed AMF experiments, the same setup was used but samples were collected at 10 min intervals before and after 10 min AMF pulsed applications, with separate pulses applied every 40 min and 4−6 pulses applied during each day of testing. In either case, at each sampling step, 3 × 200 μL samples were removed from each test tube and 600 μL fresh, 37 °C (or, for the varying incubation temperature experiments, 22 or 43 °C) 10 mM PBS was added. The

DOI: 10.1021/acsmacrolett.5b00057
ACS Macro Lett. 2015, 4, 312−316

concentration of released 4 kDa FITC-dextran in each sample collected was then measured using a fluorescence plate reader (PerkinElmer Victor3 V multilabel plate reader, 485 nm excitation/535 nm emission wavelength). The effect of the magnetic pulse on release was calculated as the percent increase in release rate between the measured value and the baseline release rate, which was determined based on a linear interpolation of the measured release rates at the two time points immediately prior to and the two points immediately after the pulse. Control gels (n = 4) were run concurrently with the pulsatile release tests using the same protocol and sampling times but without exposing the samples to the AMF.

Error and Statistical Significance. All error bars represent standard deviations ($n \geq 4$). Statistically significant differences between any pair of samples were determined using a two-tailed t test with $p < 0.05$ assuming unequal variances.

■ ASSOCIATED CONTENT

Supporting Information

Full experimental protocols and assemblies, microgel thermal characterization, SPION thermogravimetric analysis, SQUID magnetization curves and TEM images, nanocomposite degradation profiles, raw pulsatile release data, nanocomposite mechanics, and cell viability results. This material is available free of charge via the Internet at http://pubs.acs.org.

■ AUTHOR INFORMATION

Corresponding Author

*E-mail: hoaretr@mcmaster.ca.

Notes

The authors declare no competing financial interest.

■ ACKNOWLEDGMENTS

The J. P. Bickell Foundation, the Natural Sciences and Engineering Research Council of Canada (NSERC), and the Vanier Canada Graduate Scholarships Program are gratefully acknowledged for funding.

■ REFERENCES

(1) Arisaka, Y.; Kobayashi, J.; Yamato, M.; Akiyama, Y.; Okano, T. *Biomaterials* **2013**, *34*, 4214−4222.
(2) Cheng, Y.; He, C.; Ding, J.; Xiao, C.; Zhuang, X.; Chen, X. *Biomaterials* **2013**, *34*, 10338−10347.
(3) Urakami, H.; Hentschel, J.; Seetho, K.; Zeng, H.; Chawla, K.; Guan, Z. *Biomacromolecules* **2013**, *14*, 3682−3688.
(4) Bhattacharya, S.; Eckert, F.; Boyko, V.; Pich, A. *Small* **2007**, *3*, 650−657.
(5) Priimagi, A.; Cavallo, G.; Forni, A.; Gorynsztejn-Leben, M.; Kaivola, M.; Metrangolo, P.; Milani, R.; Shishido, A.; Pilati, T.; Resnati, G.; Terraneo, G. *Adv. Funct. Mater.* **2012**, *22*, 2572−2579.
(6) Jochum, F. D.; Theato, P. *Chem. Commun.* **2010**, *46*, 6717−6719.
(7) Ge, J.; Neofytou, E.; Cahill, T. J.; Beygui, R. E.; Zare, R. N. *ACS Nano* **2011**, *6*, 227−233.
(8) Holtz, J. H.; Asher, S. A. *Nature* **1997**, *389*, 829−832.
(9) Gordijo, C. R.; Koulajian, K.; Shuhendler, A. J.; Bonifacio, L. D.; Huang, H. Y.; Chiang, S.; Ozin, G. A.; Giacca, A.; Wu, X. Y. *Adv. Funct. Mater.* **2011**, *21*, 73−82.
(10) Pelton, R. H.; Chibante, P. *Colloids Surf.* **1986**, *20*, 247−256.
(11) Seo, K.; Doh, J.; Kim, D. *Langmuir* **2013**, *29*, 15137−15141.
(12) Pelton, R. *Adv. Colloid Interface Sci.* **2000**, *85*, 1−33.
(13) Dvir, T.; Timko, B. P.; Kohane, D. S.; Langer, R. *Nat. Nanotechnol.* **2011**, *6*, 13−22.
(14) Campbell, S. B.; Hoare, T. *Curr. Opin. Chem. Eng.* **2014**, *4*, 1−10.
(15) Timko, B. P.; Dvir, T.; Kohane, D. S. *Adv. Mater.* **2010**, *22*, 4925−4943.
(16) Chen, Y.-S.; Tsou, P.-C.; Lo, J.-M.; Tsai, H.-C.; Wang, Y.-Z.; Hsiue, G.-H. *Biomaterials* **2013**, *34*, 7328−7334.
(17) Fujigaya, T.; Morimoto, T.; Niidome, Y.; Nakashima, N. *Adv. Mater.* **2008**, *20*, 3610−3614.
(18) Wu, W.; Shen, J.; Banerjee, P.; Zhou, S. *Biomaterials* **2010**, *31*, 7555−7566.
(19) Zhao, X.; Wang, T.; Liu, W.; Wang, C.; Wang, D.; Shang, T.; Shen, L.; Ren, L. *J. Mater. Chem.* **2011**, *21*, 7240−7247.
(20) Brazel, C. S. *Pharm. Res.* **2009**, *26*, 644−656.
(21) Chiang, W.-H.; Ho, V. T.; Chen, H.-H.; Huang, W.-C.; Huang, Y.-F.; Lin, S.-C.; Chern, C.-S.; Chiu, H.-C. *Langmuir* **2013**, *29*, 6434−6443.
(22) Deka, S. R.; Quarta, A.; Di Corato, R.; Falqui, A.; Manna, L.; Cingolani, R.; Pellegrino, T. *Langmuir* **2010**, *26*, 10315−10324.
(23) De Las Heras Alarcon, C.; Pennadam, S.; Alexander, C. *Chem. Soc. Rev.* **2005**, *34*, 276−285.
(24) Hoare, T.; Santamaria, J.; Goya, G. F.; Irusta, S.; Lin, D.; Lau, S.; Padera, R.; Langer, R.; Kohane, D. S. *Nano Lett.* **2009**, *9*, 3651−3657.
(25) Hoffman, A. S. *Adv. Drug Delivery Rev.* **2012**, *64*, 18−23.
(26) Patenaude, M.; Campbell, S.; Kinio, D.; Hoare, T. *Biomacromolecules* **2014**, *15*, 781−790.
(27) Malda, J.; Visser, J.; Melchels, F. P.; Jüngst, T.; Hennink, W. E.; Dhert, W. J. A.; Groll, J.; Hutmacher, D. W. *Adv. Mater.* **2013**, *25*, 5011−5028.
(28) Campbell, S. B.; Patenaude, M.; Hoare, T. *Biomacromolecules* **2013**, *14*, 644−653.
(29) Hendrickson, G. R.; Lyon, L. A. *Angew. Chem., Int. Ed.* **2010**, *49*, 2193−2197.
(30) Kesselman, L. R. B.; Shinwary, S.; Selvaganapathy, P. R.; Hoare, T. *Small* **2012**, *8*, 1092−1098.
(31) Sivakumaran, D.; Maitland, D.; Hoare, T. *Biomacromolecules* **2011**, *12*, 4112−4120.
(32) Jordan, A.; Scholz, R.; Wust, P.; Schirra, H.; Schiestel, T.; Schmidt, H.; Felix, R. *J. Magn. Magn. Mater.* **1999**, *194*, 185−196.
(33) Hoare, T.; Timko, B. P.; Santamaria, J.; Goya, G. F.; Irusta, S.; Lau, S.; Stefanescu, C. F.; Lin, D.; Langer, R.; Kohane, D. S. *Nano Lett.* **2011**, *11*, 1395−1400.
(34) Patenaude, M.; Hoare, T. *Biomacromolecules* **2012**, *13*, 369−378.

DOI: 10.1021/acsmacrolett.5b00057
ACS Macro Lett. 2015, 4, 312−316